Received: 4 January 2023 | Revised: 12 April 2023 | Accepted: 19 April 2023

DOI: 10.1002/nbm.4956

SPECIAL ISSUE RESEARCH ARTICLE

NMR IN BIOMEDICINE WILEY

Electromagnetic interference elimination via active sensing and deep learning prediction for radiofrequency shielding-free MRI

Yujiao Zhao [1,2] | Linfang Xiao [1,2] | Yilong Liu [1,2] | Alex T. Leong [1,2] | Ed X. Wu [1,2]

[1]Laboratory of Biomedical Imaging and Signal Processing, The University of Hong Kong, Hong Kong, SAR, China

[2]Department of Electrical and Electronic Engineering, The University of Hong Kong, Hong Kong, SAR, China

Correspondence
Ed X. Wu, Department of Electrical and Electronic Engineering, The University of Hong Kong, Hong Kong SAR, China.
Email: ewu@eee.hku.hk

Funding information
Hong Kong Research Grant Council, Grant/Award Numbers: R7003-19, HKU17112120, HKU17127121, HKU17127022, HKU17103819, HKU17104020, HKU17127021; Lam Woo Foundation

Abstract

At present, MRI scans are typically performed inside fully enclosed radiofrequency (RF) shielding rooms, posing stringent installation requirements and causing patient discomfort. We aim to eliminate electromagnetic interference (EMI) for MRI with no or incomplete RF shielding. In this study, a method of active sensing and deep learning EMI prediction is presented to model, predict, and remove EMI signal components from acquired MRI signals. Specifically, during each MRI scan, separate EMI-sensing coils placed in various locations are utilized to simultaneously sample external and internal EMI signals within two windows (for both conventional MRI signal acquisition and EMI characterization acquisition). A convolution neural network model is trained using the EMI characterization data to relate EMI signals detected by EMI-sensing coils to EMI signals in the MRI receive coil. This model is then used to retrospectively predict and remove EMI signal components detected by the MRI receive coil during the MRI signal acquisition window. This strategy was implemented on a low-cost ultralow-field 0.055 T permanent magnet MRI scanner without RF shielding. It produced final image signal-to-noise ratios that were comparable with those obtained using a fully enclosed RF shielding cage, and outperformed existing analytical EMI elimination methods (i.e., spectral domain transfer function and external dynamic interference estimation and removal [EDITER] methods). A preliminary experiment also demonstrated its applicability on a 1.5 T superconducting magnet MRI scanner with incomplete RF shielding. Altogether, the results demonstrated that the proposed method was highly effective in predicting and removing various EMI signals from both external environments and internal scanner electronics at both 0.055 T (2.3 MHz) and 1.5 T (63.9 MHz). The proposed strategy enables shielding-free MRI. The concept is relatively simple and is potentially applicable to other RF signal detection scenarios in the presence of external and/or internal EMI.

Abbreviations: BW, bandwidth; BN, batch normalization; ETL, echo train length; EMI, electromagnetic interference; EDITER, external dynamic interference estimation and removal; FE, frequency-encoding; FSE, fast spin echo; GRE, gradient echo; NEX, number of excitations; RF, radiofrequency; ReLU, rectified linear unit; TF, spectral domain transfer function; ULF, ultralow-field.

KEYWORDS
deep learning, electromagnetic interference, electromagnetic interference elimination, electromagnetic interference prediction, electromagnetic interference sensing, MRI, radiofrequency interference, RF shielding

1 | INTRODUCTION

MRI is intrinsically superior to other medical imaging modalities (e.g., computed tomography and positron emission tomography) because it is non-invasive, nonionizing, inherently quantitative, and multiparametric.[1,2] However, conventional MRI scanners require specialized and expensive installations because of infrastructural requirements, for example, site preparation to host the large magnets that typically weigh 3000–4500 kg, magnetic and radio frequency (RF) shielding structures, electricity to drive power-consuming electronics, and water requirements for gradient cooling and cold head operation.[3] Consequently, the vast majority of clinical MRI scanners are housed inside fully enclosed RF shielding rooms on the ground floors of large hospitals and imaging centers, severely hindering the accessibility and patient-friendliness of MRI in modern healthcare.[4–9]

Consequently, there has been a growing impetus to develop MRI scanners at ultralow-field (ULF) strengths (i.e., below 0.1 T) for low-cost and/or point-of-care imaging.[9–16] At present, deep learning is expected to boost ULF image quality despite substantial MR signal level drops.[17,18] Preliminary clinical results indicated that these ULF MRI scanners produced clinically valuable information for brain pathology diagnosis.[8,9,13–16,19–21] They generally eliminate the need for a magnetic shielding cage because of dramatic fringe field reduction, yet some still require a bulky and enclosed RF shielding cage to deal with external electromagnetic interference (EMI) signals during scanning. Such RF shielding cage entails stringent installation and operation requirements, and compromises the portability and patient-friendliness of ULF MRI scanners for truly point-of-care applications (e.g., in intensive care units and surgical suites). One group used simple conductive cloth to cover the subject during scanning.[12] This method could mitigate EMI from external environments, but its performance was suboptimal. Moreover, it was probably inadequate to deal with internal EMI from low-cost ULF MRI scanner electronics such as scanner consoles, gradient/RF amplifiers, and power supplies.

Alternatively, active EMI elimination can be performed to reduce or remove EMI. Early NMR studies demonstrated that EMI signals could be significantly reduced through active EMI sensing and retrospective cancellation.[22–24] Recently, several active methods have been developed to circumvent the RF shielding cage requirement for ULF MRI.[25–30] One group utilized magnetometers to sense environmental EMI and to remove the EMI signals in the MRI receive coil via an adaptive suppression procedure.[25] This method was hardware demanding and only yielded limited success. Analytical approaches were developed to estimate EMI signals in the MRI receive coil from EMI signals detected by EMI-sensing coils using the spectral domain transfer functions among coils.[26–29] Such a concept was further extended for time domain implementation as linear convolutions and with an adaptive procedure, external dynamic interference estimation and removal, termed EDITER.[30] This method substantially eliminated EMI, and produced satisfactory brain imaging results when used together with conductive cloth and body surface electrode for EMI pickup.

Active EMI elimination is inherently based on a simple electromagnetic phenomenon, that is, the relationship between EMI signals detected by any EMI-sensing coil and the MRI receive coil can be characterized by the coupling or transfer function among two coils. In the aforementioned methods,[26–28,30] such a relationship is estimated by numerically fitting EMI-sensing coil signals to the MRI receive coil signal in the spectral or time domain. However, in realistic unshielded imaging environments, EMI behaviors and environments can be inevitably complex. For example, EMI could be emitted by various sources from external environments as well as internal scanner electronics. EMI spectral characteristics can also change dynamically because of the change in EMI sources and/or surrounding environments during scanning. These practical issues can complicate or degrade these TF-based methods, leading to inaccurate EMI signal relationship estimation.

Intuitively, a deep learning-based method can yield more effective EMI elimination in complex EMI environments, as demonstrated in our recent development of a low-cost shielding-free 0.055 T brain MRI scanner.[9] This is because a neural network model potentially offers the ability of estimating EMI signal relationships among coils using a subset of nonlinear functions instead of simple linear coefficients. In this study, we describe the details of this deep learning EMI prediction and cancellation method. Specifically, we first evaluate its effectiveness under various EMI conditions, including direct comparison with the ground truth scenario (i.e., where a fully enclosed RF shielding cage was installed). Second, we compare this method with existing analytical EMI elimination methods (i.e., spectral doamin transfer function and EDITER methods). Finally, we examine its potential applicability to high-field MRI. The results demonstrate its superior performance with regard to various and dynamically changing EMI sources on the 0.055 T brain scanner and a 1.5 T whole-body scanner with no or incomplete RF shielding.

2 | METHODS

2.1 | General framework of active sensing and deep learning EMI prediction

An EMI elimination strategy was developed to model, predict, and remove EMI signal components from acquired MRI signals by taking advantage of the well-established MRI multireceiver electronics (previously developed for parallel imaging) and the physical properties of RF signal propagation. As illustrated in Figure 1, EMI sensing coils are strategically placed around the scanner and inside an electronic cabinet to actively detect radiative EMI signals from both external environments and internal scanner electronics (Figure 1A). Within each time of repetition (TR) during scanning, the main MRI receive coil and EMI sensing coils simultaneously sample data within two acquisition windows; one is for conventional MRI signal acquisition, while the other is chosen for acquiring the EMI characterization data (containing no MRI signals due to no RF excitation, i.e., EMI signals only) (Figure 1B).

After each scan, data sampled by both the MRI receive coil and EMI sensing coils within the second window (i.e., the EMI characterization window) are used to train a convolution neural network (CNN) model that can relate the 1D temporal EMI signals received by multiple EMI sensing coils to the 1D temporal signal received by the MRI receive coil for each frequency-encoding (FE) line (Figure 1C). This model is then used to retrospectively predict the EMI signal component in the MRI receive coil signal for each FE line within the MRI signal acquisition window based on the EMI signals simultaneously detected by EMI sensing coils. Subsequently, the predicted EMI signal components are subtracted or removed from the MRI receive coil signals. This EMI prediction and removal procedure is repeated for all individual FE lines, creating EMI-free k-space data prior to any averaging and image reconstruction.

2.2 | Deep learning model implementation

A five-layer CNN model was implemented in this study. Note that each layer within the CNN model was a combination of 2D convolution, batch normalization (BN), and rectified linear unit (ReLU), except for the last layer, where only the convolution operation was performed. The kernel sizes of the five convolutional layers were 11×11, 9×9, 5×5, 1×1, and 7×7, respectively, with the corresponding number of channels being 128, 64, 32, 32, and 2. The complex EMI signals from each EMI sensing coil were processed by feeding the real and imaginary parts into the network as separate input channels. The input of the network was a 3D matrix with a size of $N_{FE} \times N_s \times 2$, where N_{FE}, N_s, and 2 are the number of points in one FE line, the number of EMI sensing coils, and the number of channels corresponding to real and imaginary parts of the raw data, respectively. The output of the network was a 2D matrix with a size of $N_{FE} \times 2$. During the training stage, the mean squared error loss (i.e., L2 loss) was minimized using an Adam optimizer[31] with $\beta 1 = 0.9$, $\beta 2 = 0.999$, and initial learning rate $= 0.0002$.

The CNN model was implemented with a batch size of 16 for 20 epochs on a Quadro RTX 8000 GPU and Intel Core i9-10900X CPU using the PyTorch 1.8.1 package on Ubuntu 18.04.5 LTS (Linux 5.4.0–77-generic). The typical training time was approximately 5 mins. Source codes can be obtained from the authors upon request or online (https://github.com/bispmri/Ultra-low-field-MRI-Scanner).

2.3 | Evaluation on a low-cost shielding-free 0.055 T brain MRI scanner

The proposed EMI elimination strategy was evaluated on a home-built shielding-free ULF 0.055 T scanner that was recently developed in our laboratory.[9] All experiments involving human subjects were approved by the local institutional board and written information consents were obtained. 3D gradient echo (GRE) and fast spin echo (FSE) sequences were implemented and optimized to demonstrate the RF shielding-free brain MRI. T1W datasets were acquired using the 3D GRE protocol with TR/TE = 52/13 ms, flip angle = 40°, sampling bandwidth (BW) = 6.25 kHz, field of view (FOV) = $250 \times 250 \times 320$ mm,[3] number of excitations (NEX) = 2, acquisition slice thickness = 10 mm, and acquisition matrix = $128 \times 128 \times 32$. T2W datasets were acquired using the 3D FSE protocol with TR/TE = 1500/202 ms, echo train length (ETL) = 21, BW = 10 kHz, FOV = $250 \times 250 \times 320$ mm^3, NEX = 2, acquisition slice thickness = 10 mm, and acquisition matrix = $128 \times 126 \times 32$.

Phantom and brain datasets were acquired with one MRI receive coil and 10 EMI sensing coils. These EMI sensing coils were deployed around and inside the scanner to detect EMI signals that were from both the external environment and those generated internally by gradient/RF electronics during scanning. Each of them was fabricated by winding 30-turn copper wire on a 3D printed coil holder (diameter = 5 cm) and was tuned to the Larmor frequency (2.32 MHz) with a BW of ~50 kHz. The detected EMI signal was passed through a two-stage preamplifier module (first stage: Gain = 30 dB; second stage: Gain = 30 dB, for input Vpp < 60 mV). The placement of these EMI-sensing coils is illustrated in Figure 1A. Three were placed in the vicinity of the patient head holder, two on each side (left and right) underneath the patient bed, and two in the vicinity of gradient and RF amplifiers inside the electronic cabinet, and one underneath the scanner.

To examine the performance of the proposed method in the presence of various and dynamically changing EMI signals, phantom imaging experiments were conducted with artificially generated EMI: (i) additional swept frequency EMI generated from a vector network analyzer (center

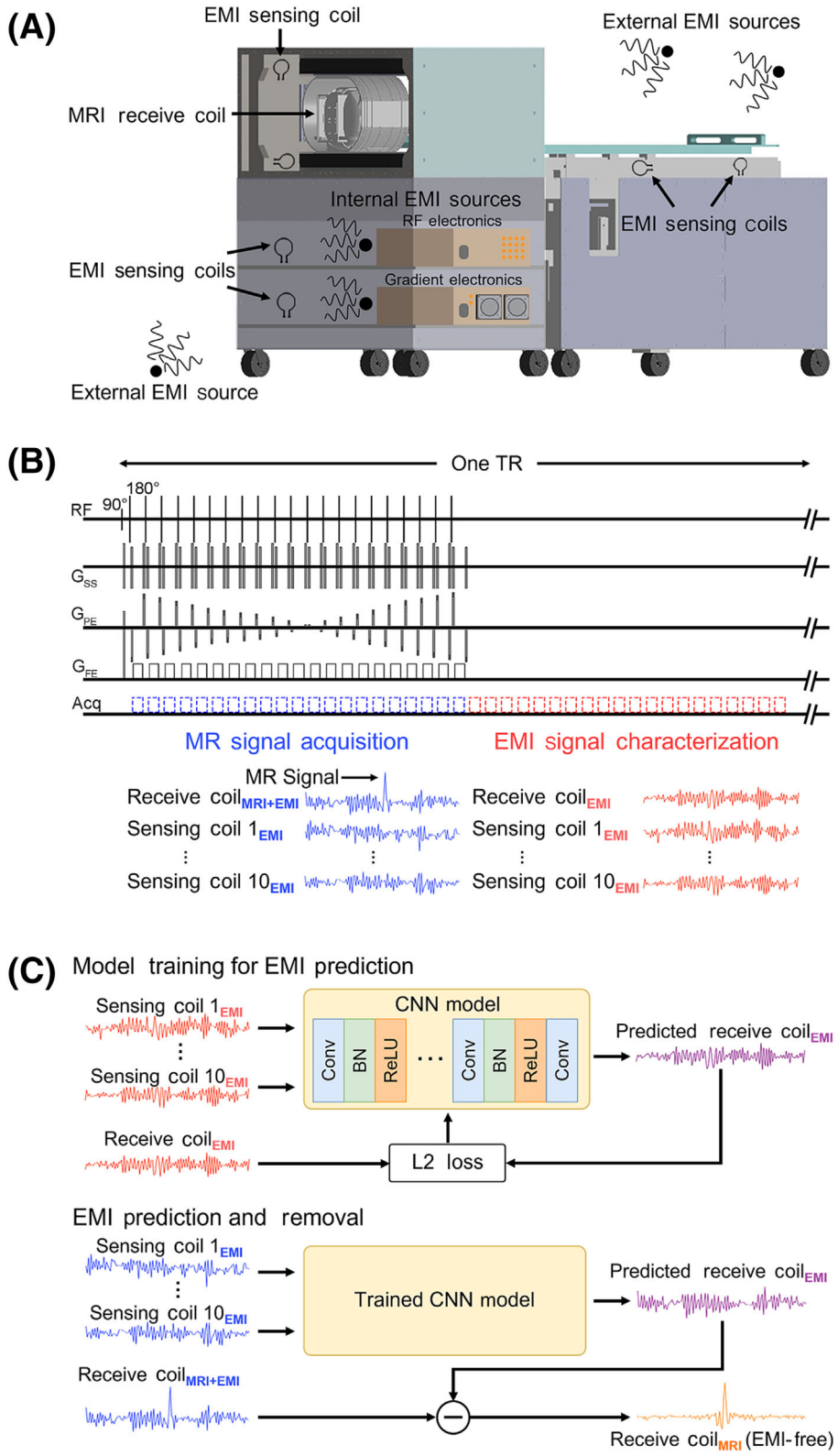

FIGURE 1 Active sensing and deep learning electromagnetic interference (EMI) prediction and cancellation on a low-cost ultralow-field (ULF) 0.055 T permanent magnet brain MRI scanner with no RF shielding, and with 2.32 MHz resonance frequency. (A) Multiple EMI-sensing coils are placed around and inside the scanner to actively detect EMI signals during MRI scanning. (B) Illustration of 3D FSE acquisition windows for MRI signal collection and EMI signal characterization. (C) A five-layer convolution neural network (CNN) model is first trained to establish the relationship between EMI signals received by the MRI receive coil and EMI-sensing coils within the second window, that is, the EMI signal characterization window. The model is then utilized to predict the EMI signal component detected by the MRI receive coil within the first window, that is, the conventional MRI signal acquisition window. BN, batch normalization; Conv, convolution; FSE, fast spin echo; ReLU, rectified linear unit; RF, radiofrequency.

FIGURE 2 Experimental setups for quantitatively assessing the effectiveness of the proposed EMI elimination method in removing EMI-related image noise/artifacts for the 0.055 T MRI scanner. For comparison, a custom-made RF shielding cage (consisting of aluminum covers) was installed to fully enclose the subject, or was removed. EMI, electromagnetic interference; RF, radiofrequency.

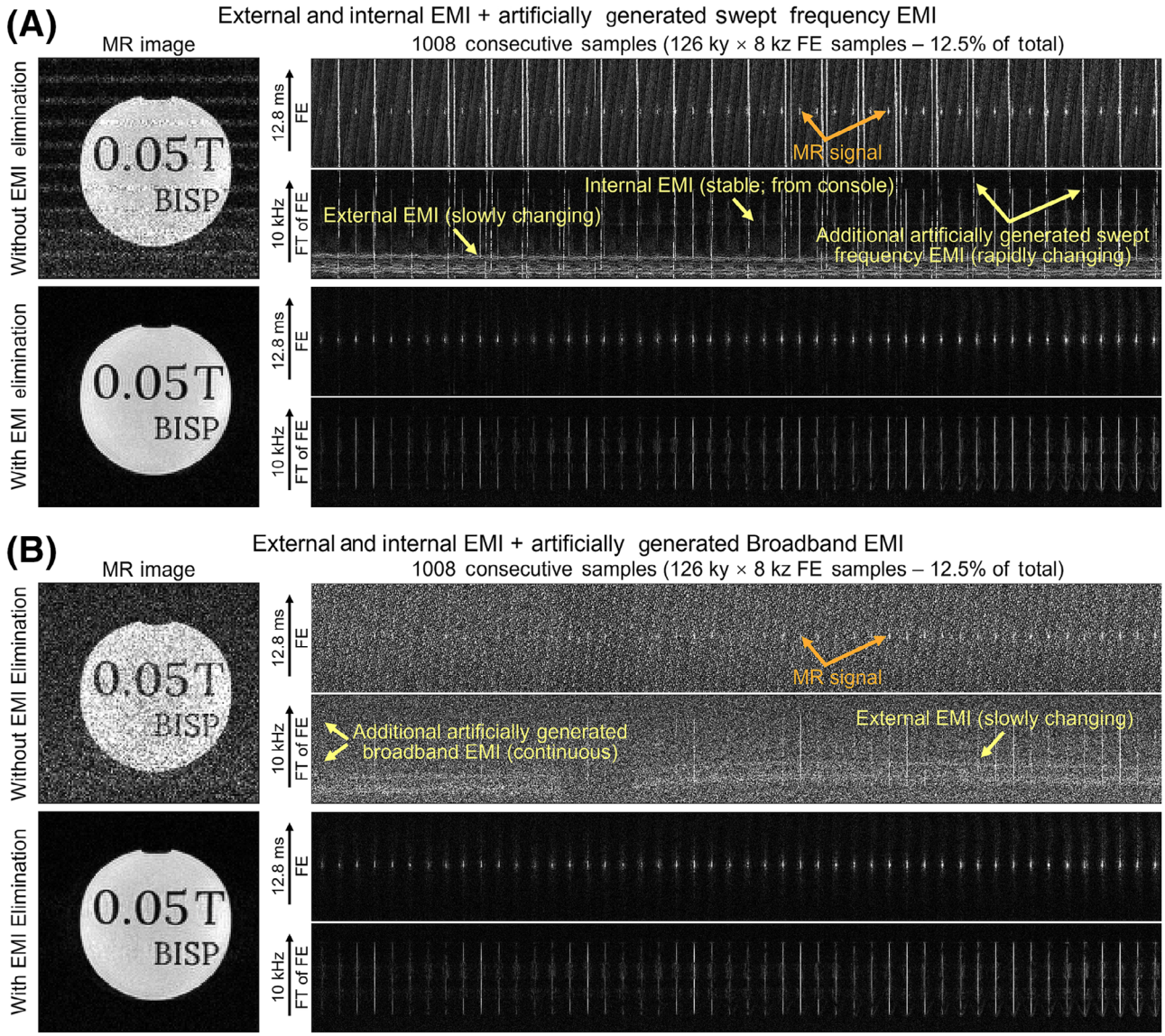

FIGURE 3 The proposed EMI elimination for shielding-free 0.055 T phantom imaging in the presence of various external and internal EMI sources. Phantom datasets were acquired using 3D FSE and with artificially generated EMI: (A) Additional swept frequency EMI generated from a nearby source, and (B) Additional broadband EMI generated from a nearby source. MR images (left) and spectral analyses (right) before and after the proposed EMI elimination are shown. The results with and without EMI elimination are displayed using the same brightness. The proposed method eliminated all EMI signals from various sources, as demonstrated by both image and spectral results. EMI, electromagnetic interference; FE, frequency-encoding; FSE, fast spin echo; FT, Fourier transform.

frequency = 2.32 MHz, sweep span = 100 kHz, frequency points = 101, and continuous sweeping cycle period = 4 s); and (ii) additional broadband EMI generated from a noise generator. The vector network analyzer or noise generator was positioned at the end of the patient bed during scanning. Then the effectiveness of the proposed method was quantitatively evaluated in human brain imaging by comparing two scenarios, where a fully enclosed RF shielding cage was installed or removed, respectively, as shown in Figure 2.

For further evaluation, the EMI elimination was performed using two existing transfer function based methods, that is, spectral domain transfer function (TF)[26–29] and EDITER.[30] TF was shown to work with data acquired within the EMI characterization window[28] or MR signal acquisition window,[29] while EDITER was developed to work with data acquired within the MR signal acquisition window.[30] In this study, TF was implemented using least squares minimization to fit EMI-sensing coil spectra to MRI receive coil spectrum for each spectral point,[28] and EDITER was implemented with the publicly available codes.[30] For direct comparison with the proposed method, TF and EDITER also used EMI characterization data for spectral and time domain TF estimation, respectively. The convolution window size and threshold value for EDITER were optimized to ensure its best performance.

2.4 | Preliminary evaluation on a 1.5 T whole-body MRI scanner

To examine the potential applicability of the proposed EMI elimination strategy to high-field MRI, the active sensing and deep learning EMI prediction strategy was applied to remove EMI signals in the phantom k-space data that were acquired on a 1.5 T scanner. Specifically, phantom datasets were acquired on a whole-body 1.5 T clinical MRI scanner using a 16-channel head array coil while the RF shielding room door was either fully closed or open. Four defective RF channels/coils within the head array coil were treated as EMI sensing coils because they detected weak MR signals but strong EMI signals (see Figure S1), thus acting as EMI-sensing coils. A 2D GRE protocol with TR/TE = 420/9 ms, BW = 25 kHz, and acquisition matrix = 200 × 200 × 20 was used.

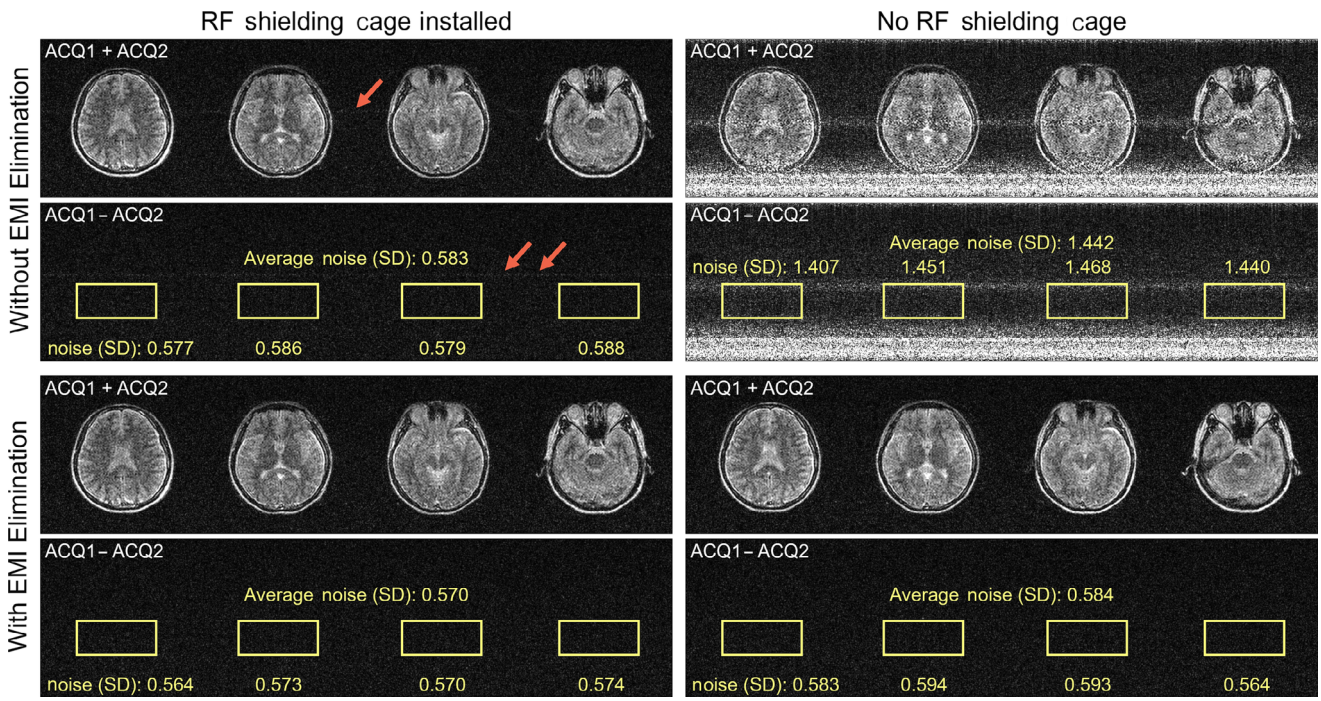

FIGURE 4 The proposed EMI elimination for shielding-free 0.055 T human brain imaging. Two brain imaging experiments (with and without the RF shielding cage) were conducted from the same normal adult subject using the 3D FSE protocol, and each with two consecutive acquisitions for noise level measurement. T2W images (average of two consecutive acquisitions, denoted as ACQ1 + ACQ2) and corresponding noise images (difference of two consecutive acquisitions, denoted as ACQ1 – ACQ2), with and without the proposed EMI elimination, are shown. Without EMI cancellation, an internal EMI signal was still present, even when the RF shielding cage was installed. With no RF shielding, both external and internal EMI signals were present. The proposed EMI cancellation method effectively eliminated external and internal EMI signals, leading to final image noise levels as low as those obtained with a fully enclosed RF shielding cage installed (within 3% range). EMI, electromagnetic interference; FSE, fast spin echo; RF, radiofrequency; SD, standard deviation.

3 | RESULTS

Figure 3 shows the EMI elimination results of shielding-free 0.055 T phantom datasets in the presence of various EMI signals. Phantom datasets were acquired using the 3D FSE protocol and with two additional artificially generated external EMI signals, that is, swept frequency EMI and broadband EMI. From the spectra of raw data (i.e., Fourier transform of FE lines) without any EMI elimination, one can easily discern and identify numerous sources of external (environmental and/or artificially generated) EMI and internal (e.g., from console) EMI, as indicated by yellow arrows. Moreover, these EMI signals were observed to be not static across the duration of each scan. For example, it can be clearly seen from the spectra (i.e., Fourier transform of FE line, or FT of FE) that spectral characteristics of some EMI sources changed dynamically, either slowly or very rapidly, during scanning. Nevertheless, the spectral and image results after EMI elimination clearly demonstrated the effectiveness of the proposed method in removing diverse and dynamically varying EMI signals.

Figure 4 compares 0.055 T shielding-free human brain imaging with the ground truth scenario (i.e., where a fully enclosed RF shielding cage was installed, as illustrated in Figure 2). Two brain imaging experiments (with and without a RF shielding cage) were conducted from the same normal adult subject using the 3D FSE protocol, and each with two consecutive acquisitions. Note that a small stable narrowband EMI noise was still present in the images without EMI elimination when the RF shielding cage was in place, caused by MRI console EMI leakage, as indicated by arrows. This indicated that the passive EMI elimination method (e.g., RF shielding cage) was sometimes inadequate to prevent the internal EMI from scanner electronics. When the RF shielding cage was removed, the brain images were severely contaminated by the internal narrowband EMI, as well as narrowband and broadband EMI from external environments. With the proposed EMI elimination strategy, these internal and external EMI-related artifacts were effectively removed.

The effectiveness of the proposed method was quantitatively examined. Here, image noise levels were calculated from the difference images between the first and second individual complex images.[32] Without the deep learning EMI elimination procedure, as expected, the average noise level without the RF shielding cage was significantly higher (1.44 in standard deviation) than that with the RF shielding cage (0.58). After deep

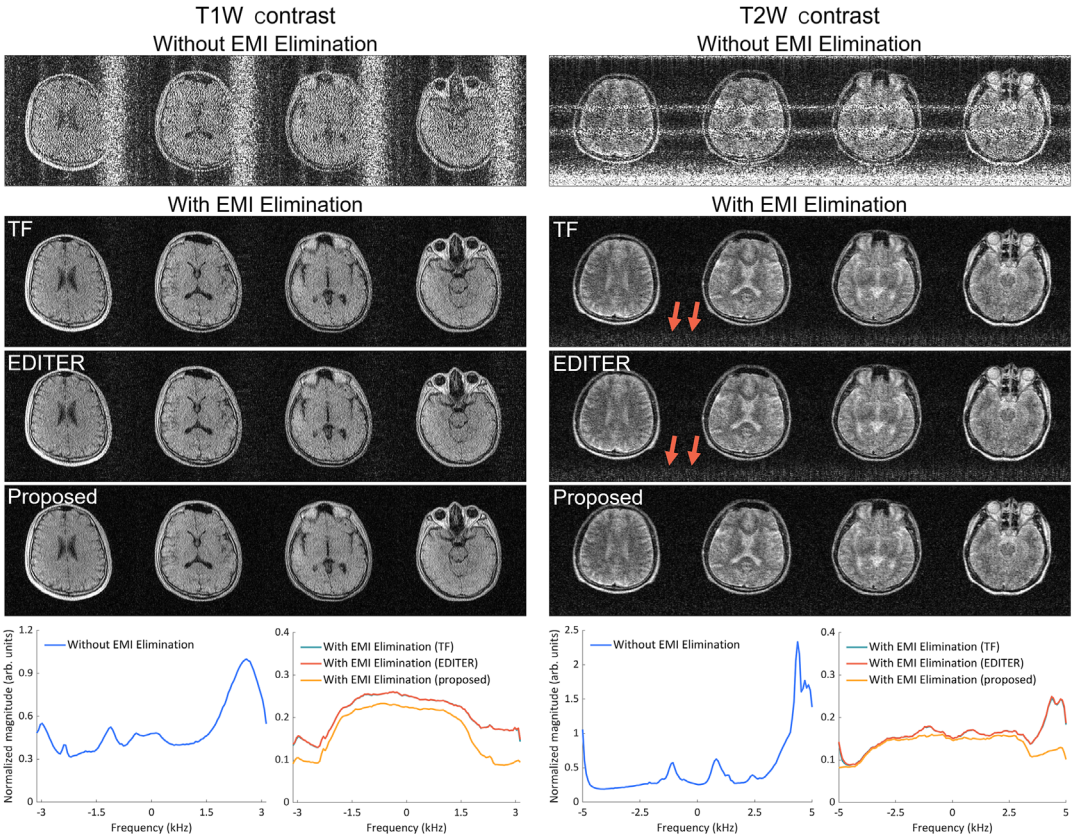

FIGURE 5 The proposed EMI elimination method versus existing methods for shielding-free 0.055 T human brain imaging with T1W and T2W contrasts. T1W and T2W brain datasets were acquired from two healthy adult subjects using 3D GRE and 3D FSE, respectively. All images are displayed at a spatial resolution of $1 \times 1 \times 5$ mm^3, while the acquisition resolution is approximately $2 \times 2 \times 10$ mm^3. The proposed deep learning EMI elimination strategy accurately predicted the EMI signal components in the MRI receive coil signals, leading to more effective EMI elimination than the existing TF and EDITER methods, as evident from both the image and spectral results. EDITER, external dynamic interference estimation and removal; EMI, electromagnetic interference; FSE, fast spin echo; GRE, gradient echo; TF, spectral domain transfer function.

learning EMI elimination, the average noise level without the RF shielding cage substantially decreased to 0.58 (from 1.42), which was only 0.2% higher than that obtained with the RF shielding cage before EMI elimination (0.58), and 2.5% higher than that after EMI elimination (0.57). The results demonstrated that, in the absence of the RF shielding cage, the proposed method was able to provide nearly complete EMI removal, producing final image noise levels as low as those obtained with a fully enclosed RF shielding cage installed (within 3% range) in human brain imaging experiments.

Figure 5 compares the proposed method with existing TF and EDITER methods for 0.055 T human brain imaging without RF shielding. T1W and T2W datasets were acquired from two normal adult subjects, respectively. Without EMI elimination, the EMI-related image artifact pattern and direction differed in T1W and T2W images because two protocols were implemented with different phase directions and BWs. With TF and EDITER, the EMI-related artifacts were substantially reduced. However, some residual EMI artifacts were still present, especially when the EMI signals were strong (as indicated by arrows in the resulting T2W images). With the proposed deep learning method, the EMI signal components in the MRI receive coil signals were more accurately predicted, resulting in more effective EMI elimination, as supported by the spectral analysis results.

Multiple EMI sensing coils are essential for effective EMI removal in complex EMI scenarios. The influence of reducing the number of EMI sensing coils on the performance of EMI elimination was examined. Figure 6 shows the results of applying EMI elimination with only one EMI sensing coil to the raw data dataset shown in Figure 3. The use of a single EMI sensing coil clearly degraded the overall EMI removal performance of the proposed method when compared with the results in Figure 3. This observation is relevant to realistic shielding-free imaging scenarios where the EMI environments are often complex, for example, when a large number of EMI sources exist. Here, the proposed method was also compared with existing TF and EDITER methods. Despite its performance degradation, it still yielded better EMI removal than TF and EDITER. This is evident from both spectral and image results, indicating that the proposed method was less sensitive to the number of EMI sensing coils.

Figure 7 illustrates the value of acquiring EMI characterization data. EMI elimination with or without using EMI characterization data (i.e., using data acquired within the MR signal acquisition window instead) was applied to the shielding-free 0.055 T phantom dataset. With EMI

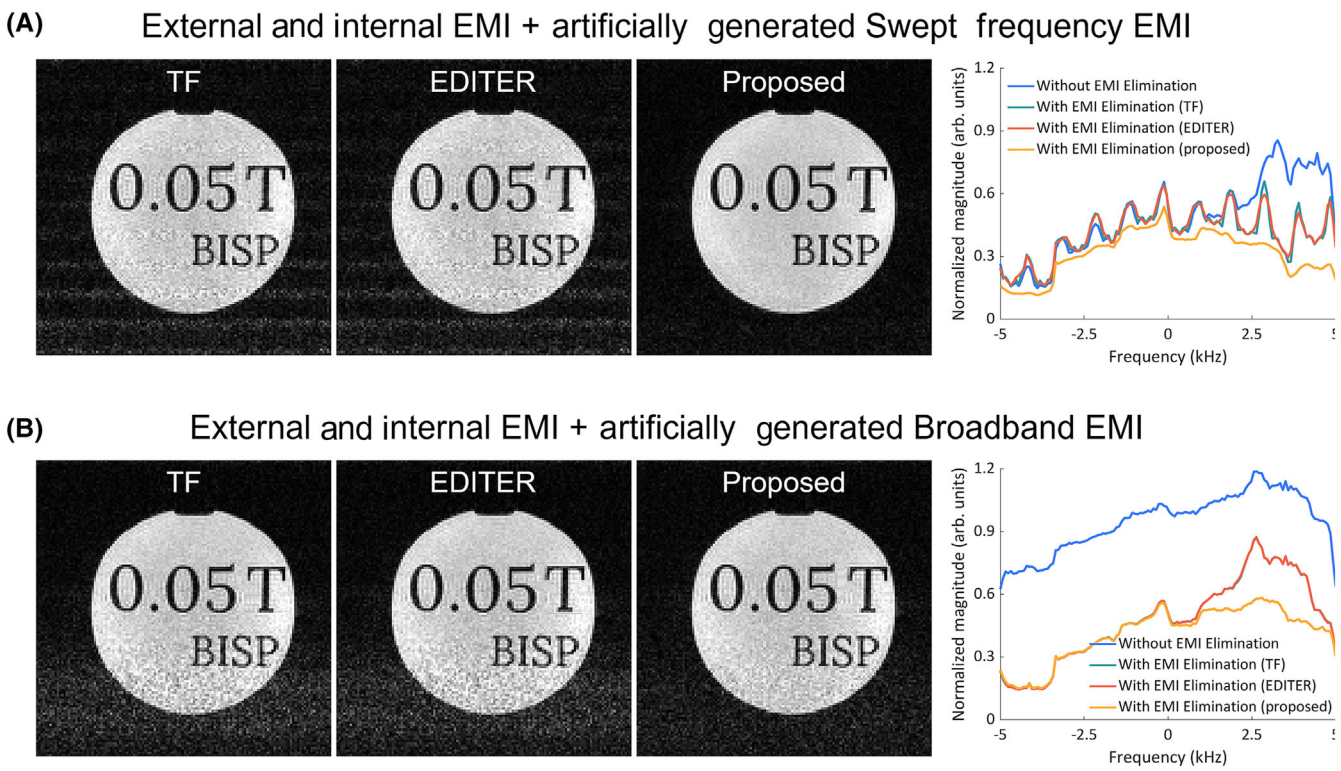

FIGURE 6 EMI elimination results of phantom datasets in Figure 3 with a reduced number of EMI sensing coils. Phantom datasets were acquired using 3D FSE and with artificially generated EMI: (A) Additional swept frequency EMI generated from a nearby source, and (B) Additional broadband EMI generated from a nearby source. EMI signals from only one EMI sensing coil were used for EMI elimination (see Figure S2 for the corresponding single EMI sensing coil signals in the time and spectral domain). The EMI elimination was also performed by existing TF and EDITER methods. With only one EMI sensing coil, distinct EMI-related artifacts were present in the TF and EDITER results, while less artifacts were present in the results using the proposed method. Magnitude-averaged spectra of all FE lines further illustrated the more effective EMI reduction performance of the proposed method. EDITER, external dynamic interference estimation and removal; EMI, electromagnetic interference; FE, frequency-encoding; TF, spectral domain transfer function.

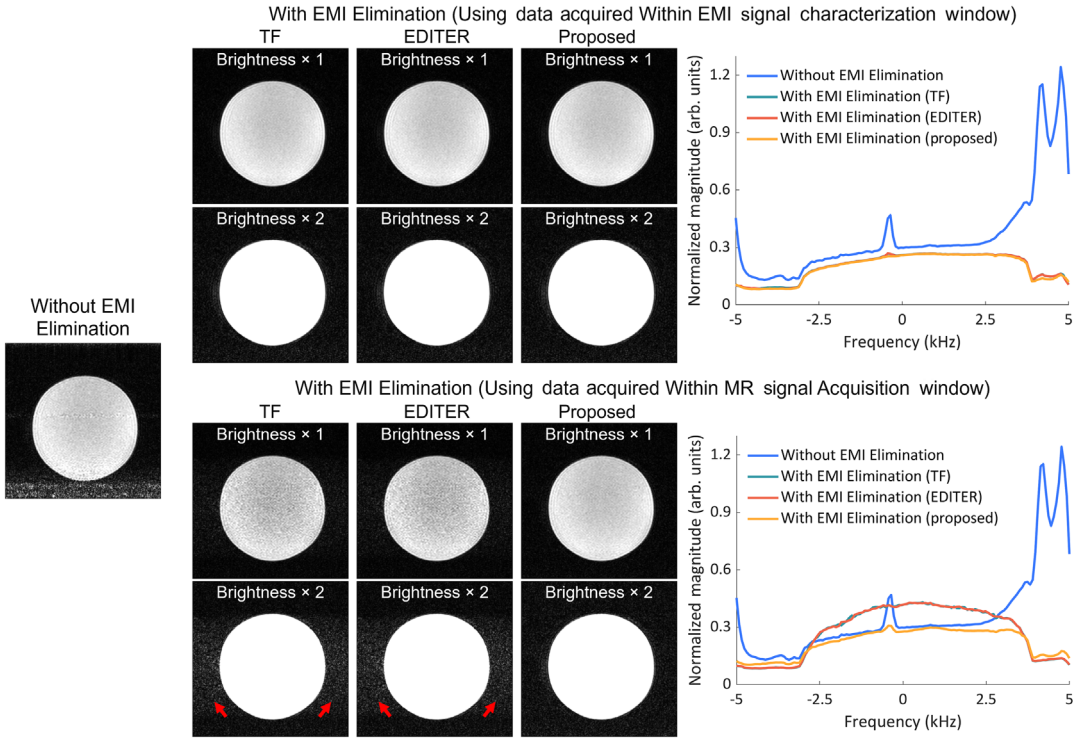

FIGURE 7 EMI elimination for shielding-free 0.055 T phantom imaging using data acquired within the EMI signal characterization window or MR signal acquisition window. The phantom dataset was acquired using 3D FSE. EMI signals from 10 EMI sensing coils were used for EMI elimination. MR images and spectral analyses before and after the EMI elimination are shown. With data acquired during the EMI signal characterization window, TF, EDITER, and the proposed method all effectively removed EMI-related artifacts. However, with data acquired during the MR signal acquisition window, the TF and EDITER results exhibited distinct residual artifacts (indicated by arrows), while the proposed EMI elimination results exhibited a slightly increased residual artifact level compared with that using EMI characterization data. These results illustrate that TF, EDITER, and the proposed EMI elimination without using EMI characterization data could lead to suboptimal performance. They also highlight the value of acquiring EMI characterization data. EDITER, external dynamic interference estimation and removal; EMI, electromagnetic interference; FSE, fast spin echo; TF, spectral domain transfer function.

characterization data, TF, EDITER, and the proposed method all effectively removed the EMI-related artifacts. However, without EMI characterization data, TF and EDITER exhibited a largely degraded EMI elimination performance, leading to apparent residual artifacts (as indicated by arrows). Such performance degradation was probably because the strong MR signals interfered with the fitting procedures in TF and EDITER. Meanwhile, the proposed method produced better image quality than TF and EDITER, with a slightly increased artifact level compared with that using EMI characterization data. These results illustrate that TF, EDITER, and the proposed EMI elimination without using EMI characterization data can lead to suboptimal performance.

Figure 8 shows the preliminary results from a 1.5 T whole-body MRI scanner sited within a fully enclosed RF shielding room. Note that, even with the RF shielding room door closed, minor EMI artifacts were still present in the images due to imperfection of the front-end electronics inside the scanner room. With the shielding room door open, as expected, more EMI artifacts were observed due to external EMI sources. Using four defective RF coils as the EMI sensing coils, the proposed method eliminated EMI artifacts arising from both hardware imperfections and incomplete RF shielding. It significantly improved the image quality when the door was open, leading to image signal-to-noise ratios (SNRs) that were generally better than those with the RF shielding room door closed. These results clearly demonstrate the potential applicability of our proposed deep learning EMI prediction concept to high-field MRI (i.e., in a high frequency regime).

4 | DISCUSSION

In this study, an EMI elimination strategy is presented to cancel EMI signal components from acquired MRI signals, thus eliminating the need for RF shielding. This method produces effective EMI removal without introducing any detriment to MRI signals. Further, the resulting image SNRs are highly comparable with those obtained using a fully enclosed RF shielding cage, indicating nearly complete EMI removal by the proposed

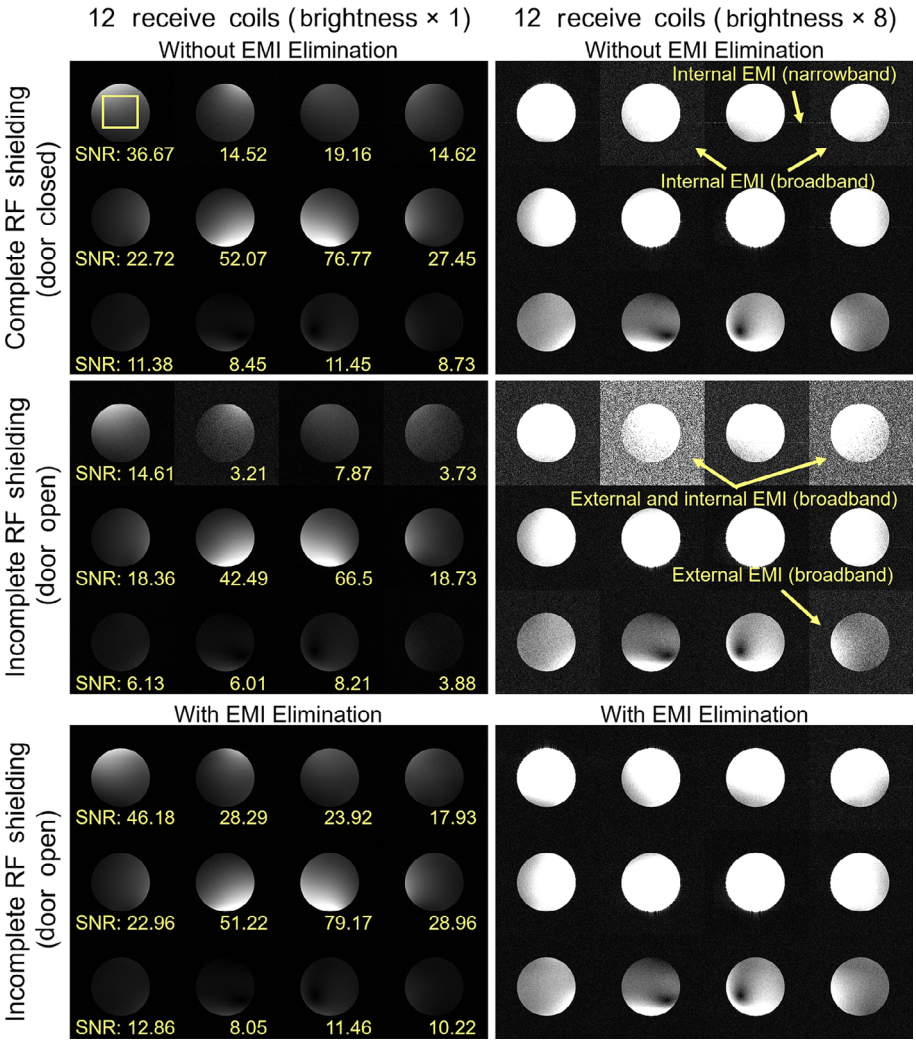

FIGURE 8 Preliminary evaluation of the proposed EMI elimination method on a clinical 1.5 T superconducting magnet whole-body MRI scanner with incomplete RF shielding (i.e., with the RF shielding room door open), with 63.9 MHz resonance frequency. The method was observed to work well, producing final phantom images with SNRs generally better than those when the RF shielding room door was closed. Images with and without EMI elimination are shown. Before EMI elimination, both narrowband and broadband internal EMI signals (generated by electronics inside the scanner room) were present even when the door was closed. The proposed strategy eliminated both external and internal EMI, and significantly improved the image quality when the door was open. The results clearly indicate the applicability of our proposed method to high-field MRI, that is, in a high frequency regime. EMI, electromagnetic interference; RF, radiofrequency; SNR, signal-to-noise ratio.

method for RF shielding-free brain MRI at 0.055 T (~2.3 MHz). The effectiveness of our proposed strategy has also been successfully demonstrated in whole-body MRI at 1.5 T (~63.9 MHz).

The prediction of EMI signals through simultaneous active EMI sensing relies on an electromagnetic phenomenon, that is, the properties of RF signal propagation among any radiative (e.g., air) and/or conductive media (e.g., surrounding EMI-emitting structures such as power lines, MRI hardware pieces and cables, and the imaging object or human body) are fully dictated by the electromagnetic coupling among these media or structures.[33,34] As revealed in recent studies,[25–28,30] such coupling relationships can be analytically characterized by spectral domain transfer functions among coils. However, in realistic unshielded imaging environments, the nature of EMI signals is diverse and complex because EMI signals from various sources (e.g., external environments and internal low-cost scanner electronics) can change dynamically during scanning. Moreover, EMI signals received by the MRI receive coil can also be influenced by the human body, which actually serves as an effective antenna[35,36] for EMI reception in a shielding-free MRI setting. Varying the body size or weight or changing position can alter the level and characteristics of EMI signals picked up by the body and subsequently detected by the MRI receive coil. As a result, transfer functions among coils can change during scanning, which may compromise the performance of existing transfer function based EMI elimination methods.

Given the above complex EMI behaviors and the nature of deep learning modeling, our proposed approach is expected to offer a more versatile strategy that can more robustly establish the relationships among EMI signals detected by EMI sensing coils and the MRI receive coil.

On one hand, a CNN model that incorporates linear convolution functions potentially offers the capability of modeling the linear EMI signal relationship among coils. On the other hand, a CNN model inherently allows nonlinear estimation of the EMI signal relationship. Note that nonlinearity and baseline noise can exist in the EMI propagation chain.[37] As illustrated in previous parallel imaging studies,[38,39] a simple CNN model yielded a more accurate estimation of the MRI signal relationship among multiple receive coils compared with conventional analytical methods. This was explained as that the signal relationship, although linear in theory, could be better approximated in practice through nonlinear functions with few degrees of freedom. Further, given that the proposed method directly derives the neural network model from scan-specific EMI characterization data, it is expected to be more resilient to the dynamically varying EMI. These hypotheses have been well supported by our 0.055 T imaging results. Successful phantom and human brain imaging (of a cohort of ~100 normal volunteers and patients) on this 0.055 T scanner have demonstrated that the proposed EMI elimination strategy worked effectively for external and internal EMI from various sources, even when the EMI sources and their spectral characteristics changed dynamically during scanning (Figure 3), outperforming existing TF and EDITER methods (Figures 5 and 6).

The implementation of the proposed method is relatively simple. Unlike most data-driven deep learning methods, the proposed method does not require a large training dataset from historical scans. In this work, the model architecture and parameters (e.g., kernel size and number of layers) were empirically determined to provide a balance between computation time and accurate EMI signal prediction. As a result, the model training converged fast (e.g., 5 and 2 min for 0.055 T and 1.5 T datasets in this study, respectively) and achieved effective EMI elimination.

There are a few research directions for future studies to pursue. First, the model was trained in this study with scan-specific EMI characterization data acquired during the deadtime of each TR (Figure 1B). Future study may utilize outer k-space data acquired within the MR signal acquisition window to train the CNN model so as to eliminate the need for dedicated EMI characterization data acquisition. Note that, on the other hand, the use of EMI characterization data could indeed improve the TF and EDITER performance in some scenarios, especially when the MR signal magnitude in k-space is strong (Figure 7). Second, the model architecture and parameters can be further optimized, for example, with explainable AI tools.[40,41] Such tools can help understand the learned model, thus offering the possibility of designing more robust models and strategies to predict EMI signals or directly extract EMI-free MR signals for truly RF shielding-free MRI in complex EMI conditions (i.e., in the presence of very strong EMI sources or their changing locations). Third, future studies may also explore the training of EMI prediction models using data collected from fewer EMI sensing coils. Finally, although promising, the 1.5 T phantom imaging experiments in the current study were simple. Future studies shall conduct more experiments and analyses with well-controlled EMI sources and dedicated EMI sensing coils to evaluate the performance of the proposed method in high-field MRI with no or incomplete RF shielding.

It is noteworthy to mention the potentially broad applications of the proposed EMI deep learning prediction strategy for retrospective EMI cancellation. The current study demonstrates that it works on an RF shielding-free mobile 0.055 T scanner (at ~2.3 MHz) and a whole-body 1.5 T scanner that operates at much higher RF frequency (~63.9 MHz). The proposed strategy is potentially applicable to other RF signal detection applications. Future studies may evaluate such an EMI elimination scheme for non-MRI RF signal detection applications (e.g., radio astronomy or radar), where we anticipate improvements by the proposed EMI elimination approach over conventional EMI mitigation methods,[42–44] especially when near and/or far field EMI characteristics and/or environments become complex.

5 | CONCLUSION

This study presents an active sensing and deep learning EMI cancellation strategy to model, predict, and remove EMI signals from acquired MRI signals. It utilizes the well-established MRI multireceiver electronics as well as the physical properties of RF signal propagation, robustly establishing the relationships among EMI signals detected by EMI sensing coils and the MRI receive coil via a relatively simple CNN model in a data-driven manner. The proposed strategy may also offer a novel concept for other RF signal detection applications in the presence of complex external and/or internal EMI emissions beyond MRI.

ACKNOWLEDGMENTS

This study is supported in part by the Hong Kong Research Grant Council (R7003-19, HKU17112120, HKU17127121, and HKU17127022 to E.X.W. and HKU17103819, HKU17104020, and HKU17127021 to A.T.L.), and the Lam Woo Foundation.

ORCID

Yujiao Zhao https://orcid.org/0000-0001-8063-887X
Yilong Liu https://orcid.org/0000-0001-9295-7982
Alex T. Leong https://orcid.org/0000-0003-1633-0445
Ed X. Wu https://orcid.org/0000-0001-5581-1546

REFERENCES

1. Fuchs VR, Sox HC Jr. Physicians' views of the relative importance of thirty medical innovations. *Health Aff*. 2001;20(5):30-42. doi:10.1377/hlthaff.20.5.30
2. Reimer P, Parizel PM, Meaney JFM, Stichnoth FA. *Clinical MR imaging: a practical approach*. Springer; 2010. doi:10.1007/978-3-540-74504-4
3. Webb AG. *Magnetic resonance technology: hardware and system component design*. Royal Society of Chemistry; 2016:402. doi:10.1039/9781782623878
4. Geethanath S, Vaughan JT. Accessible magnetic resonance imaging: a review. *J Magn Reson Imaging*. 2019;49(7):e65-e77. doi:10.1002/jmri.26638
5. Marques JP, Simonis FFJ, Webb AG. Low-field MRI: an MR physics perspective. *J Magn Reson Imaging*. 2019;49(6):1528-1542. doi:10.1002/jmri.26637
6. Wald LL, McDaniel PC, Witzel T, Stockmann JP, Cooley CZ. Low-cost and portable MRI. *J Magn Reson Imaging*. 2020;52(3):686-696. doi:10.1002/jmri.26942
7. Sarracanie M, Salameh N. Low-field MRI: how low can we go? A fresh view on an old debate. *Front Physiol*. 2020;8:172. doi:10.3389/fphy.2020.00172
8. Arnold TC, Freeman CW, Litt B, Stein JM. Low-field MRI: clinical promise and challenges. *J Magn Reson Imaging*. 2023;57(1):25-44. doi:10.1002/jmri.28408
9. Liu Y, Leong ATL, Zhao Y, et al. A low-cost and shielding-free ultra-low-field brain MRI scanner. *Nat Commun*. 2021;12(1):1-14. doi:10.1038/s41467-021-27317-1
10. Sarracanie M, LaPierre CD, Salameh N, Waddington DEJ, Witzel T, Rosen MS. Low-cost high-performance MRI. *Sci Rep*. 2015;5:15177. doi:10.1038/srep15177
11. Cooley CZ, McDaniel PC, Stockmann JP, et al. A portable scanner for magnetic resonance imaging of the brain. *Nat Biomed Eng*. 2021;5(3):229-239. doi:10.1038/s41551-020-00641-5
12. O'Reilly T, Teeuwisse WM, de Gans D, Koolstra K, Webb AG. In vivo 3D brain and extremity MRI at 50 mT using a permanent magnet Halbach array. *Magn Reson Med*. 2021;85(1):495-505. doi:10.1002/mrm.28396
13. Wu EX, Liu Y, Leong ATL, et al. A shielding-free ultra-low-field 0.055T brain MRI scanner for accessible healthcare. In: Proceedings of the 31st Annual Meeting of ISMRM; 2022:4371.
14. Leong ATL, Liu Y, Zhao Y, et al. A feasibility study of 0.055T MRI for neuroimaging and comparison with clinical 3T MRI. In: Proceedings of the 31st Annual Meeting of ISMRM; 2022:4370.
15. He Y, He W, Tan L, et al. Use of 2.1 MHz MRI scanner for brain imaging and its preliminary results in stroke. *J Magn Reson*. 2020;319:106829. doi:10.1016/j.jmr.2020.106829
16. Sheth KN, Mazurek MH, Yuen MM, et al. Assessment of brain injury using portable, low-field magnetic resonance imaging at the bedside of critically ill patients. *JAMA Neurol*. 2021;78(1):41-47. doi:10.1001/jamaneurol.2020.3263
17. Iglesias JE, Schleicher R, Laguna S, et al. Quantitative brain morphometry of portable low-field-strength MRI using super-resolution machine learning. *Radiology*. 2023;306(3):e220522. doi:10.1148/radiol.220522
18. Lau V, Xiao L, Zhao Y, et al. Pushing the limits of low-cost ultra-low-field MRI by dual-acquisition deep learning 3D super-resolution. *Magn Reson Med*. 2023;1-17. doi:10.1002/mrm.29642
19. Yuen MM, Prabhat AM, Mazurek MH, et al. Portable, low-field magnetic resonance imaging enables highly accessible and dynamic bedside evaluation of ischemic stroke. *Sci Adv*. 2022;8(16):eabm3952. doi:10.1126/sciadv.abm3952
20. Mazurek MH, Cahn BA, Yuen MM, et al. Portable, bedside, low-field magnetic resonance imaging for evaluation of intracerebral hemorrhage. *Nat Commun*. 2021;12(1):5119. doi:10.1038/s41467-021-25441-6
21. Mazurek MH, Yuen MM, Cahn BA, et al. Low-field, portable magnetic resonance imaging at the bedside to assess brain injury in patients with severe COVID-19. *Neurology*. 2021;96(15 Supplement):1349.
22. Trushkin D, Shushakov O, Legchenko A. The potential of a noise-reducing antenna for surface NMR ground-water surveys in the earth's magnetic field. *Geophys Prospect*. 1994;42(8):855-862. doi:10.1111/j.1365-2478.1994.tb00245.x
23. Walsh DO. Multi-channel surface NMR instrumentation and software for 1D/2D groundwater investigations. *J Appl Geophys*. 2008;66(3–4):140-150. doi:10.1016/j.jappgeo.2008.03.006
24. Mueller-Petke M, Yaramanci U. Improving the signal-to-noise ratio of surface-NMR measurements by reference channel based noise cancellation. In: Near surface 2010-16th EAGE European Meeting of Environmental and Engineering Geophysics; 2010: p cp-164-00002.
25. Huang X, Dong H, Qiu Y, et al. Adaptive suppression of power line interference in ultra-low field magnetic resonance imaging in an unshielded environment. *J Magn Reson*. 2018;286:52-59. doi:10.1016/j.jmr.2017.11.009
26. Rearick T, Charvat GL, Rosen MS, Rothberg JM. Noise suppression methods and apparatus patent. US Patent No 9,797,971; 2017.
27. Srivinas SA, Cooley CZ, Stockmann JP, McDaniel PC, Wald LL. Retrospective electromagnetic interference mitigation in a portable low field MRI system. In: Proceedings of the 28th Annual Meeting of ISMRM; 2020:1269.
28. Dyvorne H, Rearick T, Poole M, et al. Freeing MRI from its Faraday cage with interference rejection. In: Proceedings of the 29th Annual Meeting of ISMRM; 2021:0749.
29. Yang L, He W, He Y, Wu J, Shen S, Xu Z. Active EMI suppression system for a 50 mT unshielded portable MRI scanner. *IEEE Trans Biomed Eng*. 2022;69(11):3415-3426. doi:10.1109/TBME.2022.3170450
30. Srinivas SA, Cauley SF, Stockmann JP, et al. External dynamic interference estimation and removal (EDITER) for low field MRI. *Magn Reson Med*. 2022;87(2):614-628. doi:10.1002/mrm.28992
31. Kingma DP, Ba J. Adam: a method for stochastic optimization. In: 3rd International Conference on Learning Representations (ICLR), San Diego, CA, USA; 2015.
32. Xie VB, Lyu M, Wu EX. EPI Nyquist ghost and geometric distortion correction by two-frame phase labeling. *Magn Reson Med*. 2017;77(5):1749-1761. doi:10.1002/mrm.26251
33. Ferrara E, Widrow B. Multichannel adaptive filtering for signal enhancement. *IEEE Trans Circ Syst*. 1981;28(6):606-610. doi:10.1109/TCS.1981.1085009

34. Briggs F, Bell J, Kesteven M. Removing radio interference from contaminated astronomical spectra using an independent reference signal and closure relations. *Astron J*. 2000;120(6):3351-3361. doi:10.1086/316861
35. Kibret B, Teshome AK, Lai DT. Analysis of the human body as an antenna for wireless implant communication. *IEEE Trans Antennas Propag*. 2016; 64(4):1466-1476. doi:10.1109/TAP.2016.2526070
36. Sen S, Maity S, Das D. The body is the network: to safeguard sensitive data, turn flesh and tissue into a secure wireless channel. *IEEE Spectrum*. 2020; 57(12):44-49. doi:10.1109/MSPEC.2020.9271808
37. Zanche ND. RF receivers: signal detection chain, digitization, system noise figures—from MRI signal to bits. In: Proceedings of the 27th Annual Meeting of ISMRM; 2018.
38. Akçakaya M, Moeller S, Weingärtner S, Uğurbil K. Scan-specific robust artificial-neural-networks for k-space interpolation (RAKI) reconstruction: database-free deep learning for fast imaging. *Magn Reson Med*. 2019;81(1):439-453. doi:10.1002/mrm.27420
39. Zhang C, Moeller S, Demirel OB, Uğurbil K, Akçakaya M. Residual RAKI: a hybrid linear and non-linear approach for scan-specific k-space deep learning. *Neuroimage*. 2022;256:119248. doi:10.1016/j.neuroimage.2022.119248
40. Lipton ZC. The mythos of model interpretability: in machine learning, the concept of interpretability is both important and slippery. *Queue*. 2018; 16(3):31-57. doi:10.1145/3236386.3241340
41. Miller T. Explanation in artificial intelligence: insights from the social sciences. *Artif Intell*. 2019;267:1-38. doi:10.1016/j.artint.2018.07.007
42. Raza J, Boonstra A-J, Van der Veen A-J. Spatial filtering of RF interference in radio astronomy. *IEEE Signal Proc Lett*. 2002;9(2):64-67. doi:10.1109/97.991140
43. Jeffs BD, Li L, Warnick KF. Auxiliary antenna-assisted interference mitigation for radio astronomy arrays. *IEEE Trans Signal Processing*. 2005;53(2): 439-451. doi:10.1109/TSP.2004.840787
44. Huang Y, Liao G, Zhang L, Xiang Y, Li J, Nehorai A. Efficient narrowband RFI mitigation algorithms for SAR systems with reweighted tensor structures. *IEEE Trans Geosci Remote Sens*. 2019;57(11):9396-9409. doi:10.1109/TGRS.2019.2926440

SUPPORTING INFORMATION

Additional supporting information can be found online in the Supporting Information section at the end of this article.

How to cite this article: Zhao Y, Xiao L, Liu Y, Leong AT, Wu EX. Electromagnetic interference elimination via active sensing and deep learning prediction for radiofrequency shielding-free MRI. *NMR in Biomedicine*. 2023;e4956. doi:10.1002/nbm.4956